ISSN 1990-3413, Astrophysical Bulletin, 2019, Vol. 74, No. 4, pp. 365–378. © Pleiades Publishing, Ltd., 2019.
Russian Text © The Author(s), 2019, published in Astrofizicheskii Byulleten', 2019, Vol. 74, No. 4, pp. 374–387.

Galaxy Clusters and Their Outskirts: the "Red Sequence", Star Formation Rate, Stellar Mass

F. G. Kopylova[1]* and A. I. Kopylov[1]

[1]*Special Astrophysical Observatory, Russian Academy of Sciences, Nizhnii Arkhyz, 369167 Russia*

Received October 3, 2018; revised February 28, 2019; accepted February 28, 2019

Abstract—We study the nearest outskirts ($R < 3R_{200c}$) of 40 groups and clusters of galaxies of the local Universe ($0.02 < z < 0.045$ and 300 km s^{-1} $< \sigma <$ 950 km s^{-1}). Using the SDSS DR10 catalog data, we determined the stellar mass of galaxy clusters corresponding to K_s-luminosity (which we determined earlier based on the 2MASX catalog data) $(M_*/M_\odot) \propto (L_K/L_\odot)^{1.010\pm0.004}$ ($M_K < -21\overset{\mathrm{m}}{.}5$, $R < R_{200c}$). We also found the dependence of the galaxy cluster stellar mass on halo mass: $(M_*/M_\odot) \propto (M_{200c}/M_\odot)^{0.77\pm0.01}$. Our results show that the fraction of galaxies with quenched star formation ($M_K < -21\overset{\mathrm{m}}{.}5$) is maximal in the central regions of the galaxy clusters and equals, on the average, 0.81 ± 0.02; it decreases to 0.44 ± 0.02 outside of the projected radius $R_{\rm sp}$ ($2 < R/R_{200c} < 3$), which we found from the observed profile, but still remains higher than that in the field by 27%. The fraction of early-type "red sequence" galaxies decreases from 0.54 ± 0.02 in the center to 0.24 ± 0.01 beyond $R_{\rm sp}$, reaching its field value.

DOI: 10.1134/S1990341319040035

Key words: *galaxies: clusters—galaxies: star formation—galaxies: evolution*

1. INTRODUCTION

It is known from observations that the high-density central virialized regions of galaxy groups and clusters are populated by massive red early-type galaxies without star formation (see, e.g., [1–3]). It has also been established that the properties of galaxies in a cluster are related not only to the positions of the galaxies in it, but also to the time of their entry into the system (see, e.g., [4–6]). Model orbits of galaxies that fall within the gravitational potential of galaxy clusters can be found in [7–9]. The changes in the properties of galaxies in groups and clusters with increasing distance from the center have been investigated in many studies. The main result is the discovery of a decreasing star formation rate in galaxies in the direction of the cluster center (e.g., [10–13]). It was shown that after a certain time, star formation fades in all galaxies of the system [8]. If galaxies with star formation are occasionally found, then they have either entered the cluster recently, or are not members at all but are merely projected onto the region.

The authors of [11] found that the decrease in the fraction of galaxies with star formation is observed up to $5R_{200}$. To explain this effect, model simulations were performed for the (N-body) star formation rate change along the galaxy cluster radius. They showed that a considerable fraction of galaxies beyond the virial cluster radius have once been in their central regions—up to 50% within 1–2 $R_{\rm vir}$ [11, 14].

The physical mechanisms that are present in the dense inner medium of the clusters lead to a decrease in the amount of gas in the galaxies and, in turn, to a decrease in the star formation rate. The key mechanism leading to the venting of gas and a decrease in the efficiency of the star formation process is assumed to be the influence of AGN feedback in the clusters [15]. Over the course of several Gyr, galaxies may lose the gaseous envelope even in the vicinity of galaxy clusters [16]. Or, if the density of the cluster environment is sufficiently high, the cool gas disc can be stripped off as a result of ram pressure [17, 18].

Another hypothesis explains the quenching of star formation in the vicinity of galaxy clusters by the fact that galaxies in the groups that fall into the cluster have already undergone pre-processing, having lost their gas as a result of the process described above (see, e.g., [12, 13, 19, 20]).

In order to establish the variation along the normalized system radius (up to $3R/R_{200}$) of the fraction of early-type "red sequence" galaxies and the specific star formation rate, we used in our study a sample

*E-mail: flera@sao.ru

of 40 galaxy groups and clusters with registered X-ray emission, including systems of galaxies from the Leo and Hercules supercluster regions, as well as several nearby systems: clusters A 1367, A 1656 and eight groups of galaxies considered earlier in [21]. The sample is formed in such a way that it would cover a maximum range of radial velocity dispersions of the galaxy systems from 300 km s^{-1} to 950 km s^{-1} in the local Universe ($0.02 < z < 0.045$). The results for six rich systems of galaxies from the studied sample have already been published in our paper [22].

In this work, we used data from the following catalogs: SDSS[1] [23] (Sloan Digital Sky Survey) Data Release 10, 2MASS (2MASX, Two-Micron ALL-Sky Survey Extended Source Catalog[2] [24]), and NED[3] (NASA Extragalactic Database).

The paper is organized as follows. In Section 2 we describe the procedure of selecting the outskirts of the galaxy groups and clusters (in units of radii R_{200c} and $R_{\rm sp}$). In Section 3 we present the constructed color–magnitude sequence for early-type galaxies in the systems of galaxies and determine the fraction of early-type galaxies. Section 4 describes our measurements of the total stellar mass of the system of galaxies within the radius R_{200c} and compares the obtained stellar mass with the dynamical mass determined earlier. In Section 5 we give the distributions of the specific star formation rate of the clusters with fixed galaxy stellar mass and without such. We show variations of the fraction of quenched galaxies (QG) along the normalized radius of the systems with fixed galaxy stellar mass and without such, and for comparison we estimate the fractions of field galaxies with quenched star formation. In the Conclusions we list the main results. In this work we used the following cosmological parameters: $\Omega_m = 0.3$, $\Omega_\Lambda = 0.7$, $H_0 = 70$ km s^{-1} Mpc^{-1}.

2. THE NEAREST OUTSKIRTS OF GALAXY GROUPS AND CLUSTERS

We determined the dynamical characteristics of the studied systems of galaxies: radial velocity, radial velocity dispersion, cluster mass (halo)—in the regions of radius R_{200c} (in projection). The R_{200c} radius is the radius of a sphere within which the density in the system exceeds the critical density of the Universe by a factor of 200. It is determined by the radial velocity dispersion of the system galaxies [22]. Model simulations often use another radius, R_{200m}—the radius of a sphere within which the density in the system is over 200 times the average density of the Universe.

The relations between the obtained masses M_{200c} and K_s-luminosity (2MASX), as well as the mass–luminosity ratio and the dynamical parameters (based on SDSS DR7, DR8 data) for the galaxy groups and clusters under study are presented in our earlier papers [25–27].

In our study, it is important to isolate the nearest outskirts of the galaxy systems: in addition to the radius R_{200c}, we must determine the "splashback" radius $R_{\rm sp}$ ($R_{\rm sp} > R_{200c}$). We analyze the distributions which characterize in detail the structure and kinematics of each system, and present as figures the following:

1) the deviation of the radial velocities of cluster member galaxies and background galaxies from the average radial velocity of the cluster or group as a function of squared radius (the distance to the cluster center);

2) the integral distribution of the total number of galaxies as a function of squared radius;

3) the position of the galaxies on the sky plane in equatorial coordinates;

4) the histogram of the distribution of the radial velocities of all galaxies within the radius R_{200c}. As an example, we show in Figs. 1a–1d such graphs for MKW 04.

Let us consider Fig. 1b, where we present the projected cluster profile. As the distance from the cluster center increases, we observe first a sharp increase in the number of galaxies, and then, beyond the limits of the virialized region [27], its linear growth (shown in the figure by a straight line). The radius of the virialized region R_{200c} and the radius $R_{\rm sp}$ are shown by the dashed and dashed and dotted lines. Note that $R_{\rm sp}$ corresponds to the distance from the center where the sharp increase in the number of cluster members changes to linear. In the bottom of this figure we also show the distribution of early-type galaxies brighter than $M_K = -21\overset{\rm m}{.}5$, which we used to refine the radius. Such galaxies are usually located in the central virialized regions of galaxy systems. We assume that the radius $R_{\rm sp}$ corresponds to the apocenter of the orbits for galaxies that entered the virialized region of the cluster and then flew out to come back again. In other words, it separates the galaxies which enter the cluster for the first time from those that are already cluster members.

According to model (N-body) simulations [28], the maximum separation of the galaxies from the clusters does not exceed 1–2.5 $R_{\rm vir}$. Model simulations for the dark halo profile of the clusters [30] have

[1] \http://www.sdss.org

[2] http://www.ipac.caltech.edu/2mass/releases/allsky/

[3] \http://nedwww.ipac.caltech.edu

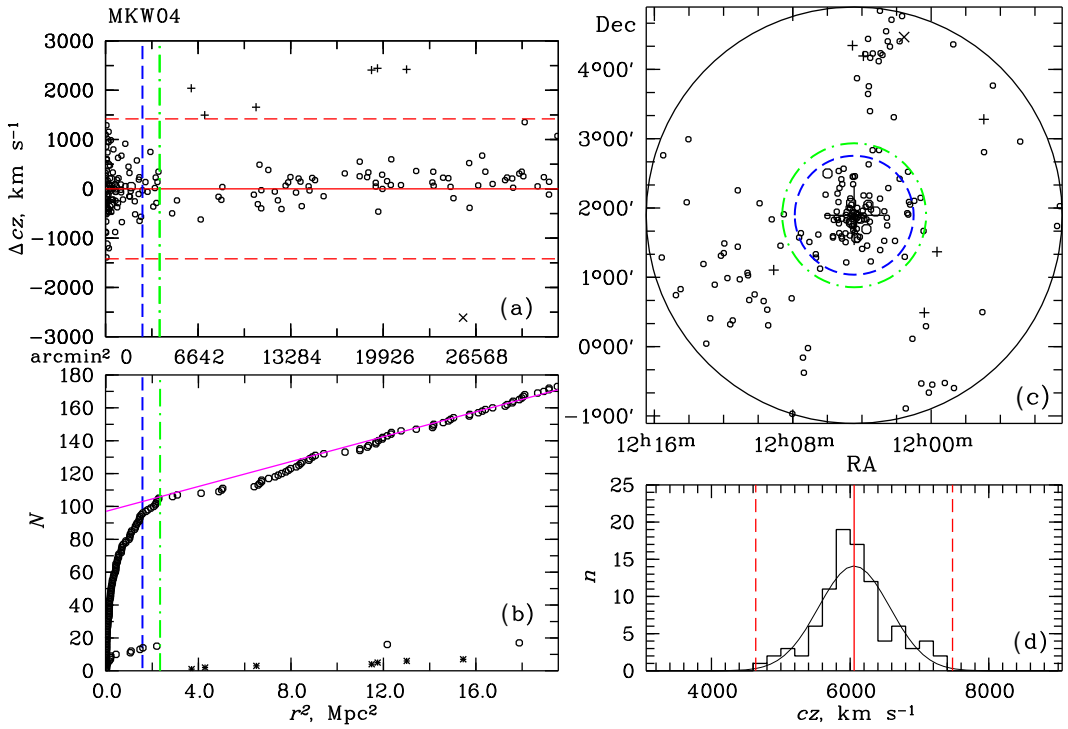

Fig. 1. Distribution of galaxies in the MKW 04 cluster. (a) deviation of galaxy radial velocities from the average radial velocity of the cluster, determined from the galaxies within the radius R_{200c}. The horizontal dashed lines correspond to deviations $\pm 2.7\sigma$, the vertical dashed line shows the radius R_{200c}, and the dashed and dotted line represents radius $R_{\rm sp}$. The larger circles denote galaxies brighter than $M_K^* = -24^{\rm m}$, the straight crosses mark the background galaxies, the diagonal crosses show the foreground galaxies. (b) integral distribution of the total number of galaxies (upper curve) as a function of squared distance to the group center. The lower points correspond to early-type galaxies brighter than $M_K < -21\overset{\rm m}{.}5$. The circles correspond to the galaxies marked by circles in panel (a), and the stars show the background galaxies. The dashed and dotted line shows the radius $R_{\rm sp}$. (c) sky distribution in equatorial coordinates for galaxies shown in panel (a) (the designations are the same). The circles mark regions with the radius R_{200c} (dashes) and radius $R_{\rm sp}$ (dashes and dots). The region under study is restricted by a circle with the radius equal to $3.5\,R_{200c}$ (solid line). The center of the cluster is marked by a large cross. (d) radial velocity distribution for all the galaxies within the radius R_{200c} (the Gaussian (solid curve) corresponding to the velocity dispersion of the group is shown for the cluster members). The solid vertical line shows the average radial velocity of the group, and the dashed lines correspond to deviations of $\pm 2.7\sigma$.

shown that for rapidly accreting halos, the galaxy cluster radius where a sharp increase occurs in the slope of the halo surface density distribution is in the 0.8–1.0 R_{200m} interval, and in the $R_{\rm sp} \sim 1.5\ R_{200m}$ range for slowly accreting halos.

Based on observation of nearby groups of the Local Universe, the authors of [31] derived the radius $R_{\rm sp} \approx 1.33 R_{200c}$, calling it "the second turnaround radius". For distant galaxies, the $R_{\rm sp}$ radii were found based on the SDSS catalog data from the galaxy surface density profile and from the mass profile determined by weak gravitational lensing [32, 33]. The radius $R_{\rm sp}$ obtained by us from the integral distribution of the number of galaxies as a function of squared distance from the cluster center is equal, on average, to $(1.54 \pm 0.06)\ R_{200c}$ for 40 studied systems, which amounts to $0.96 \pm 0.04\ R_{200m}$ (considering that $4R_{200c} \approx 2.5R_{200m}$). This value is larger than the estimate in [31], but agrees with the results derived from model simulations, for example [30].

The physical properties of the groups and clusters of galaxies considered in this work for the region of radius R_{200c} are presented in the columns of Table 1: (1) name of the galaxy cluster; (2) radial velocity dispersion with the cosmological correction $(1+z)^{-1}$; (3)–(5) radii R_{200c}, R_{200m}, and $R_{\rm sp}$ in Mpc; (6) number of galaxies for which the redshift and radial velocity dispersion are known; (7) measured redshift; (8) halo mass M_{200c} determined from σ, with an error that corresponds to the σ measurement error; (9) $L_{K,200c}$–luminosity with the error determined in the same way; (10) stellar mass $M_{*,200c}$ with the error approximately the same as that for the luminosity. stellar mass determination is described in detail in Section 4.

Table 1. Physical properties of galaxy clusters

Cluster	σ, km s^{-1}	R_{200c}, Mpc	R_{200m}, Mpc	$R_{\rm sp}$, Mpc	N_z	z_h	M_{200c}, $10^{14}\,M_\odot$	$L_{K,200c}$, $10^{12}\,M_\odot$	$M_{*,200c}$, $10^{12}\,M_\odot$
(1)	(2)	(3)	(4)	(5)	(6)	(7)	(8)	(9)	(10)
A 2147	853 ± 46	2.076	3.32	3.64	344	0.036179	10.57 ± 1.71	12.68 ± 0.6	11.34
A 2063	753 ± 62	1.833	2.93	2.68	146	0.034664	7.28 ± 1.80	5.97 ± 0.4	5.78
A 1367	749 ± 47	1.835	2.94	2.78	249	0.021743	7.21 ± 1.46	7.62 ± 0.2	7.25
A 2199	746 ± 44	1.820	2.91	3.61	288	0.030458	7.09 ± 1.25	9.88 ± 0.3	8.84
A 1185	676 ± 52	1.692	2.70	2.97	177	0.032883	5.70 ± 1.28	6.68 ± 0.2	6.16
MKW 03s	608 ± 67	1.474	2.36	1.95	82	0.044953	3.81 ± 1.26	4.56 ± 0.4	4.60
NGC 6338	552 ± 61	1.348	2.16	2.12	83	0.029342	2.87 ± 0.94	2.75 ± 0.1	2.52
NGC 6107	546 ± 55	1.332	2.13	1.90	99	0.031093	2.78 ± 0.84	3.45 ± 0.1	3.62
RXJ 1722	524 ± 86	1.269	2.03	1.64	37	0.046580	2.44 ± 1.20	3.58 ± 0.6	3.92
MKW 04	515 ± 54	1.263	2.02	1.53	91	0.020208	2.34 ± 0.74	2.50 ± 0.1	2.57
UGC 04991	515 ± 68	1.256	2.01	1.72	58	0.031958	2.33 ± 0.92	2.26 ± 0.2	2.06
A 1983	460 ± 47	1.115	1.78	1.67	97	0.044803	1.65 ± 0.51	4.86 ± 0.6	4.50
MKW 08	450 ± 44	1.100	1.76	1.73	103	0.026906	1.56 ± 0.46	3.08 ± 0.1	3.10
NGC 5098	445 ± 58	1.083	1.73	1.73	58	0.036812	1.50 ± 0.59	2.81 ± 0.1	3.21
RBS 858	445 ± 63	1.081	1.73	1.64	50	0.039586	1.51 ± 0.64	2.37 ± 0.2	2.29
NGC 2795	425 ± 61	1.039	1.66	1.33	49	0.028887	1.31 ± 0.56	2.08 ± 0.02	1.80
MKW 04s	423 ± 56	1.033	1.65	1.53	56	0.027928	1.29 ± 0.51	1.83 ± 0.1	1.78
VV 196	412 ± 69	1.003	1.60	1.16	36	0.035289	1.19 ± 0.60	1.29 ± 0.05	1.16
RXJ 1033	411 ± 65	0.996	1.59	1.48	40	0.045170	1.18 ± 0.56	2.23 ± 0.2	2.21
AWM 1	402 ± 58	0.982	1.57	1.15	48	0.028652	1.11 ± 0.48	2.29 ± 0.1	1.92
AWM 4	380 ± 62	0.927	1.48	1.34	37	0.031827	0.94 ± 0.46	1.49 ± 0.1	1.40
NGC 7237	376 ± 52	0.919	1.47	1.47	52	0.026102	0.91 ± 0.38	1.53 ± 0.1	1.52
NGC 3158	375 ± 61	0.918	1.47	1.24	38	0.022630	0.90 ± 0.44	1.74 ± 0.1	1.70
RXC J1511	374 ± 76	0.909	1.45	1.22	24	0.038990	0.89 ± 0.54	1.22 ± 0.1	0.98
NGC 5171	371 ± 52	0.908	1.47	1.47	51	0.023000	0.88 ± 0.37	1.46 ± 0.1	1.23
NGC 3119	355 ± 59	0.867	1.39	1.20	36	0.029657	0.76 ± 0.38	1.50 ± 0.1	1.71
A 1228B	347 ± 66	0.842	1.35	1.28	28	0.042892	0.71 ± 0.40	1.74 ± 0.1	1.48
A 2162	346 ± 61	0.844	1.35	1.12	32	0.032147	0.71 ± 0.37	1.44 ± 0.1	1.58
NGC 2783	346 ± 58	0.848	1.36	1.02	35	0.022151	0.71 ± 0.38	1.07 ± 0.1	1.04
A 1177	337 ± 66	0.822	1.32	1.14	26	0.032159	0.65 ± 0.35	1.20 ± 0.1	1.14
NGC 6098	335 ± 77	0.817	1.31	1.14	19	0.030936	0.64 ± 0.44	0.87 ± 0.1	0.95
UGC 07115	334 ± 46	0.818	1.31	1.06	53	0.022199	0.64 ± 0.26	1.29 ± 0.1	1.18
NGC 2832	331 ± 43	0.810	1.30	1.20	60	0.023044	0.62 ± 0.24	1.59 ± 0.1	1.03
NGC 5627	314 ± 55	0.768	1.23	1.10	33	0.026682	0.53 ± 0.28	1.34 ± 0.1	1.18

2.1. Comments on Some Galaxy Clusters

In the galaxy cluster pair A 2199 + A 2197, A 2199 is a richer system with a higher X-ray luminosity [26]. Both clusters are projected close to each other on the celestial sphere and have practically identical radial velocities. A 2197 is separated by approximately 79 arc minutes in δ from A 2199 and, according to our measurements, is located within the $R_{\rm sp}$ radius of cluster A 2199, i.e., has common outskirts with A 2199. Therefore, in our work the cluster A 2197 is not considered individually.

In the galaxy cluster pair A 2147 + A 2151, A 2147 is also a richer system with a higher X-ray luminosity [26]. These clusters are located close to each other in celestial sphere projection and have practically identical radial velocities. However, cluster A 2151 is located further, approximately 105 arc minutes by δ from A 2147. Although according to our measurements A 2151 does not coincide with the $R_{\rm sp}$ radius of A 2147, we also do not consider it separately, since both clusters have common outskirts.

3. THE "RED SEQUENCE" OF GALAXY GROUPS AND CLUSTERS

Early type galaxies are the brightest, and therefore, the most massive members of galaxy clusters. There are located for the most part in the central virialized regions (see, e.g., [34]). Thus, according to our estimates, in the clusters of the Hercules supercluster they account for about 60–70% of galaxies brighter than $M_K = -23\overset{\rm m}{.}3$ [21]. The fact that early type galaxies are the brightest objects in the clusters is also confirmed by the luminosity functions for early- and late-type galaxies presented in the paper.

One of the fundamental relations for early type galaxies is the dependence of color on magnitude, which has a slight scatter for groups and clusters of galaxies and forms the so-called "red sequence" (RS). The RS is related to the physical properties of the systems: its shape characterizes the mass–metallicity relation, and its scatter shows the galaxy age variations (see, e.g., [35]). The early-type galaxy RS is often used in search activities. It can usually be used to find galaxy clusters in the near [36–38] and far Universe [39–43]. In this work, we used early type RS galaxies brighter than $M_K = -21\overset{\rm m}{.}5$ in order to study in more detail the outskirts of the galaxy clusters under investigation ($R < 3R_{200c}$).

We used the following criteria in our selection of galaxies: $fracDeV \geq 0.8$, where $fracDeV$ is a galaxy parameter which represents the input of the bulge into the total luminosity of the galaxy, based on the SDSS r-band catalog data; $c = r_{90}/r_{50} \geq 2.6$, where c is the concentration index, equal to the ratio of radii that limit 90% and 50% of the Petrosian fluxes. Additionally, we imposed a color restriction for $u - r$: $\Delta(u - r) > -0.2$, which follows from the obtained dependence of the $u - r$ color on the Petrosian magnitude for the galaxy clusters, e.g., the Hercules supercluster: $u - r = -0.078 \times r_{\rm Pet} + 3.81$ with $2\sigma = -0.2$.

For the studied systems, we constructed a series of figures similar to the ones in Fig. 2 for the galaxy clusters MKW 04 and MKW 04s. Figs. 2a and 2d show the color–magnitude diagrams with the "red sequence". Early-type galaxies on the RS that satisfy the $-0.075 < g - r < 0.075$ condition are shown by filled circles. Figs. 2b–2f show the projected phase-space diagrams for the galaxy clusters MKW 04 and MKW 04s, where $\Delta V/\sigma$ is the ratio of the difference of the galaxy radial velocity and the average radial velocity of the cluster to the radial velocity dispersion of the cluster, and R/R_{200c} is the distance of the galaxy from the selected cluster center normalized to radius R_{200c}.

The projected phase-space diagram shows the dependence between the distance of the galaxy from the selected center and its usually normalized radial velocity. Based on the positions of the galaxies on the diagram one can investigate, for example, the variations of star formation in the clusters, and also make conclusions about galaxies belonging to the "old" population of the galaxy cluster or to galaxies that have fallen into it only recently, of the those that have already flew out of the virialized region ("splashback"-galaxies) [4–9]. Analyzing the position of a galaxy on the phase-space diagram, one can conveniently study the history of its accretion into the group or cluster.

As the galaxy system center we used the coordinates of the brightest galaxy which is usually located not far from the center of the X-ray emitting region. If there are several bright galaxies or the bright galaxy is shifted from the galaxy concentration center, then the x-ray emitting center or the galaxy centroid are usually taken as the center. Fig. 2 shows only the galaxies brighter than $M_K = -21\overset{\rm m}{.}5$. In panels (b)–(f) we used the tilted dashed lines to separate the mostly virialized galaxies from those that fall into the cluster for the first time (model simulations were taken from [45]).

Note that the main bulk of early-type RS galaxies is located in the central regions of the galaxy clusters, within the derived radius $R_{\rm sp}$. At the same time, a small portion of galaxies may also be located at a distance of $3R_{200c}$, in accordance with model simulations, e.g., [12]. We found that the fraction of early-type RS galaxies decreases, based on the all-system average, by a factor of two: from

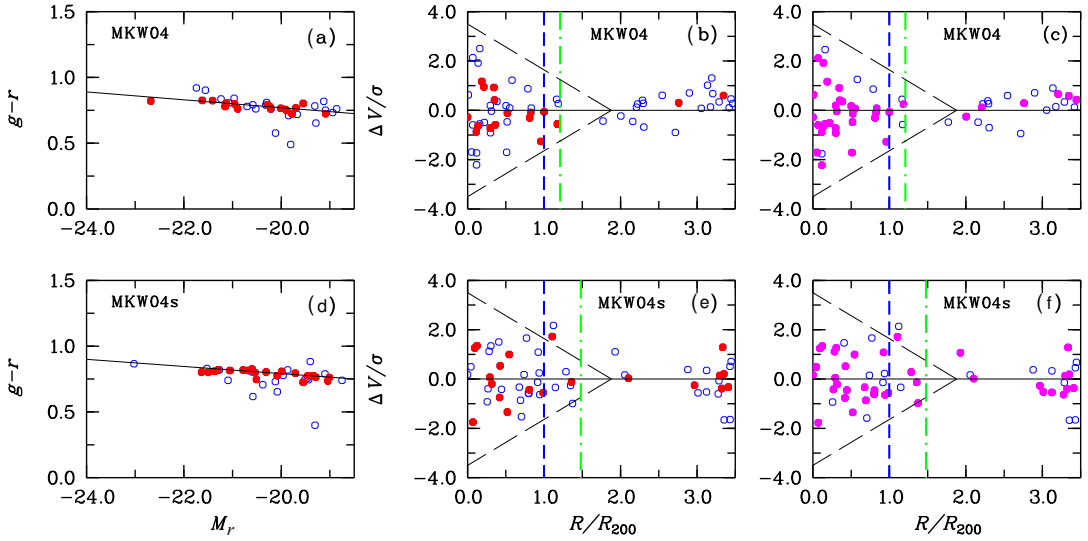

Fig. 2. (a) and (d): "color–absolute magnitude" dependence ($M_K < -21\overset{\text{m}}{.}5$) for galaxy clusters MKW 04 and MKW 04s correspondingly. The filled circles show early type galaxies of the "red sequence". (b) and (e): phase-space diagram: velocity of galaxy clusters MKW 04 and MKW 04s as a function of radius. The velocity is determined as the ratio of the difference between the radial velocities of the galaxies and the average radial velocity of the cluster to radial velocity dispersion. The R/R_{200c} radius is the distance of the galaxy from the center, normalized to the R_{200c} radius. Early-type RS-galaxies are shown by filled circles. The dashed and dashed-and-dotted lines correspond to the R_{200c} and $R_{\rm sp}$ radii. The galaxies are selected within $\pm 2.7\sigma$ [44]. (c) and (f): same phase-space diagrams, but with the filled circles showing galaxies with quenched star formation ($\log sSFR[\mathrm{Gyr}^{-1}] < -1.75$).

0.54 ± 0.02 in the central regions to 0.24 ± 0.02 in $2R/R_{200c} < R < 3R/R_{200c}$. Beyond the $R_{\rm sp}$ radii the fraction of early type galaxies $frac_E$ also amounts to 0.24 ± 0.01, on average. The results of $frac_E$ determination along the normalized radius of the studied system are presented in Table 2. Column (1) gives the name of the system, and the remaining columns give the variation ranges for radii (R/R_{200c} and $R_{\rm sp}$).

In our paper [22] we considered two regions between the superclusters Hercules and Leo, free of galaxy clusters (practically field), and derived that the two-field average for the fraction of early-type galaxies brighter than $M_K = -21\overset{\text{m}}{.}5$ is equal to 0.24 ± 0.01. Unlike the cluster galaxies, early type galaxies in these regions (field galaxies) are not closely positioned on the RS, although they also demonstrate a color–magnitude dependence (Fig. 3).

As we derived above, for the nearest outskirts of galaxy clusters $2 < R/R_{200c} < 3$ and $R > R_{\rm sp}$ the average fractions are 0.24 ± 0.02 and 0.24 ± 0.01 (Table 2), i.e. they are not different from $\langle frac_E \rangle$ for field galaxies. Within the radius $1 < R/R_{200c} < 2$ the average fraction of early type galaxies is higher than in the field, and is equal to 0.31 ± 0.01. Thus, the main portion of early type galaxies in the cluster lies within the limits of the radius $R_{\rm sp}$ determined from observations: some of them are already virialized, others (according to, e.g., model simulations in [9]) have left the virialized regions and, having reached the apocenter of the orbit $R_{\rm sp}$ that we found, will return into it again.

4. RELATION BETWEEN THE STELLAR MASS AND THE TOTAL MASS IN GROUPS AND CLUSTERS OF GALAXIES

In order to determine the full stellar mass of a system of galaxies within the projected radius R_{200c} for $M_K < -21\overset{\text{m}}{.}5$ we used the results of stellar mass data for galaxies from the SDSS DR10 archive which were obtained by fitting FSPS [46] models to u, g, r, i, z-band SDSS-photometry (corrected for extinction). New results on the photometry of large galaxies (brightest cluster galaxies) are presented in this release, the luminosity of which has been underestimated earlier due to excessive background

subtraction [47]. We should note that not all galaxies which we included in the sample have spectral data in SDSS DR10 (which includes stellar masses). For example, they are absent for the brightest galaxy in the A 2162, AWM 4, and A 1139 systems, the luminosity of which may account for up to 40% of the total luminosity. Only seven systems (18% of the total number) have data available on all galaxies, and the remaining galaxy systems have no stellar mass measurements (from 3% to 19%), and about 30% for systems RXJ 1722 and NGC 5627. When no stellar mass measurements were available,

Table 2. Variations of the fraction of early-type galaxies along the radius

Cluster	$(0-0.25)R/R_{200c}$	$(0-1)R/R_{200c}$	$(1-2)R/R_{200c}$	$(2-3)R/R_{200c}$	$(0-1)R_{\rm sp}$	$1R_{\rm sp}-3R/R_{200c}$
(1)	(2)	(3)	(4)	(5)	(6)	(7)
A 2147	0.45 ± 0.11	0.37 ± 0.04	0.28 ± 0.04	0.31 ± 0.04	0.34 ± 0.03	0.30 ± 0.03
A 2063	0.62 ± 0.14	0.50 ± 0.08	0.23 ± 0.07	0.28 ± 0.06	0.46 ± 0.07	0.26 ± 0.05
A 1367	0.58 ± 0.14	0.47 ± 0.07	0.32 ± 0.08	0.15 ± 0.06	0.44 ± 0.06	0.21 ± 0.06
A 2199	0.69 ± 0.15	0.46 ± 0.06	0.33 ± 0.06	0.18 ± 0.04	0.40 ± 0.04	0.18 ± 0.04
A 1185	0.49 ± 0.14	0.30 ± 0.05	0.33 ± 0.07	0.23 ± 0.07	0.32 ± 0.05	0.25 ± 0.06
MKW 03s	0.62 ± 0.22	0.49 ± 0.09	0.32 ± 0.11	0.21 ± 0.10	0.47 ± 0.08	0.22 ± 0.08
NGC 6338	0.47 ± 0.20	0.29 ± 0.09	0.26 ± 0.12	0.25 ± 0.09	0.30 ± 0.08	0.23 ± 0.08
NGC 6107	0.47 ± 0.19	0.43 ± 0.09	0.45 ± 0.14	0.14 ± 0.06	0.44 ± 0.09	0.21 ± 0.07
RXC J1722	0.50 ± 0.23	0.44 ± 0.12	0.24 ± 0.13	0.27 ± 0.15	0.42 ± 0.10	0.25 ± 0.11
MKW 04	0.33 ± 0.15	0.41 ± 0.12	0.25 ± 0.28	0.09 ± 0.09	0.40 ± 0.11	0.08 ± 0.09
UGC 04991	0.39 ± 0.17	0.35 ± 0.10	0.38 ± 0.18	0.22 ± 0.12	0.39 ± 0.10	0.21 ± 0.09
A 1983	0.54 ± 0.19	0.52 ± 0.09	0.26 ± 0.08	0.24 ± 0.12	0.45 ± 0.07	0.22 ± 0.08
MKW 08	0.54 ± 0.28	0.49 ± 0.12	0.26 ± 0.10	0.29 ± 0.11	0.43 ± 0.09	0.28 ± 0.09
NGC 5098	0.54 ± 0.25	0.46 ± 0.12	0.19 ± 0.08	0.39 ± 0.14	0.35 ± 0.08	0.37 ± 0.12
RBS 858	0.62 ± 0.28	0.46 ± 0.12	0.50 ± 0.22	0.12 ± 0.13	0.48 ± 0.12	0.29 ± 0.16
NGC 2795	0.46 ± 0.24	0.34 ± 0.13	0.21 ± 0.14	0.40 ± 0.17	0.40 ± 0.12	0.28 ± 0.11
MKW 04s	0.60 ± 0.44	0.37 ± 0.13	0.25 ± 0.36	0.50 ± 0.43	0.35 ± 0.11	0.40 ± 0.33
VV 196	0.75 ± 0.33	0.48 ± 0.17	0.06 ± 0.06	0.36 ± 0.19	0.41 ± 0.14	0.23 ± 0.10
RXC J1033	0.67 ± 0.30	0.38 ± 0.11	0.26 ± 0.11	0.13 ± 0.10	0.34 ± 0.08	0.20 ± 0.11
AWM 1	0.33 ± 0.27	0.39 ± 0.14	0.33 ± 0.17	0.42 ± 0.22	0.40 ± 0.14	0.36 ± 0.14
AWM 4	0.70 ± 0.34	0.43 ± 0.08	0.10 ± 0.10	0.14 ± 0.06	0.39 ± 0.07	0.05 ± 0.05
NGC 7237	0.46 ± 0.24	0.39 ± 0.12	0.36 ± 0.19	0.25 ± 0.28	0.39 ± 0.10	0.20 ± 0.22
NGC 3158	0.50 ± 0.25	0.48 ± 0.10	0.14 ± 0.15	–	0.46 ± 0.09	–
RXC J1511	0.57 ± 0.21	0.58 ± 0.12	0.27 ± 0.18	0.36 ± 0.21	0.54 ± 0.10	0.33 ± 0.16
NGC 5171	0.31 ± 0.09	0.40 ± 0.07	0.33 ± 0.17	0.22 ± 0.17	0.39 ± 0.06	0.20 ± 0.15
NGC 3119	0.67 ± 0.35	0.28 ± 0.06	0.11 ± 0.08	–	0.24 ± 0.04	0.07 ± 0.07
A 1228B	0.50 ± 0.25	0.35 ± 0.14	0.28 ± 0.14	0.50 ± 0.27	0.33 ± 0.11	0.40 ± 0.19
A 2162	0.43 ± 0.30	0.43 ± 0.17	0.36 ± 0.19	0.38 ± 0.25	0.45 ± 0.15	0.29 ± 0.16
NGC 2783	0.29 ± 0.12	0.27 ± 0.07	0.40 ± 0.33	0.60 ± 0.44	0.29 ± 0.07	0.50 ± 0.31
A 1177	0.71 ± 0.27	0.55 ± 0.12	0.50 ± 0.27	0.50 ± 0.43	0.52 ± 0.10	0.57 ± 0.36
NGC 6098	0.67 ± 0.61	0.30 ± 0.20	0.20 ± 0.22	–	0.21 ± 0.14	0.50 ± 0.61
UGC 07115	0.40 ± 0.33	0.57 ± 0.18	0.29 ± 0.23	–	0.54 ± 0.16	–
NGC 2832	0.50 ± 0.35	0.39 ± 0.08	0.47 ± 0.19	0.60 ± 0.31	0.42 ± 0.07	0.56 ± 0.23
NGC 5627	0.29 ± 0.23	0.21 ± 0.12	0.40 ± 0.24	0.17 ± 0.18	0.27 ± 0.11	0.22 ± 0.17
Total $N = 40$	0.54 ± 0.04	0.44 ± 0.02	0.31 ± 0.01	0.24 ± 0.02	0.42 ± 0.02	0.24 ± 0.01

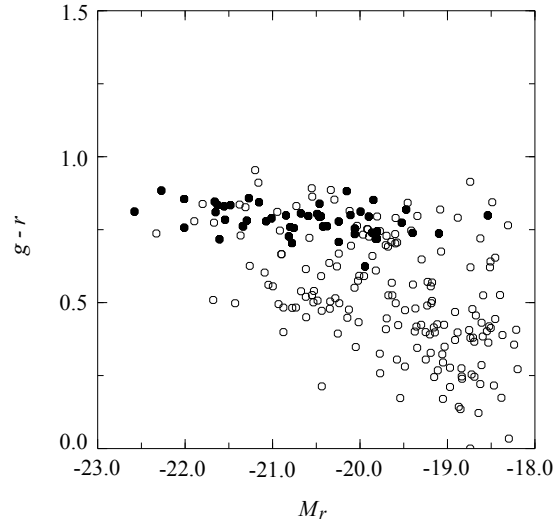

Fig. 3. Color–absolute magnitude dependence for the field galaxies in the region with the center $14^{\rm h}.5$, 35° and a $300'$ radius ($M_K < -21^{\rm m}.5$, $0.030 < z < 0.045$). Early type galaxies are shown by filled circles.

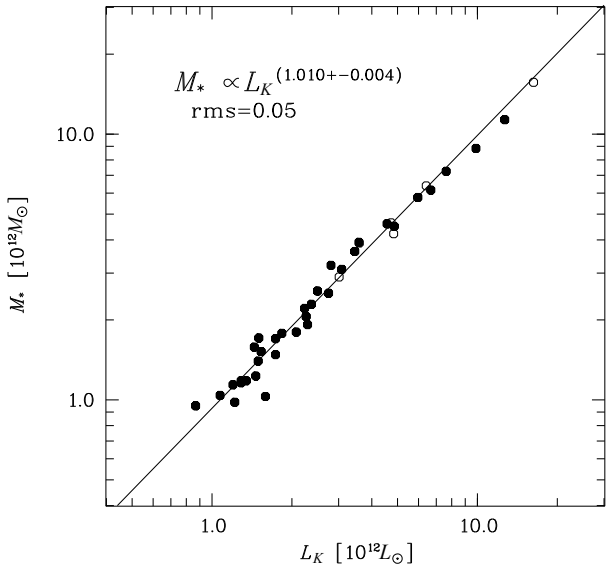

Fig. 4. Dependence of the galaxy cluster stellar mass on K_s-luminosity within R_{200c}. The line corresponds to the regression ratio $M_*/M_\odot \propto (L_K/L_\odot)^{1.010\pm0.004}$. The empty circles show the galaxy clusters from [22].

we estimated then approximately from the $u-r$ and $g-r$ colors, magnitudes, and the $fracDeV$ parameter.

In our earlier papers [21, 25, 27] we used the 2MASX catalog data to determine the K_s-luminosities of the considered galaxy clusters within R_{200c} (corresponding to $M_K < -21^{\rm m}.0$). The mass of the star population of the galaxies is best determined from these luminosities. It can be derived by taking into account the mass–luminosity ratio for spiral and elliptical galaxies. We compared the derived K_s–luminosities with the stellar masses presented in SDSS DR10 and obtained for our sample of 40 galaxy groups and clusters the following relation:

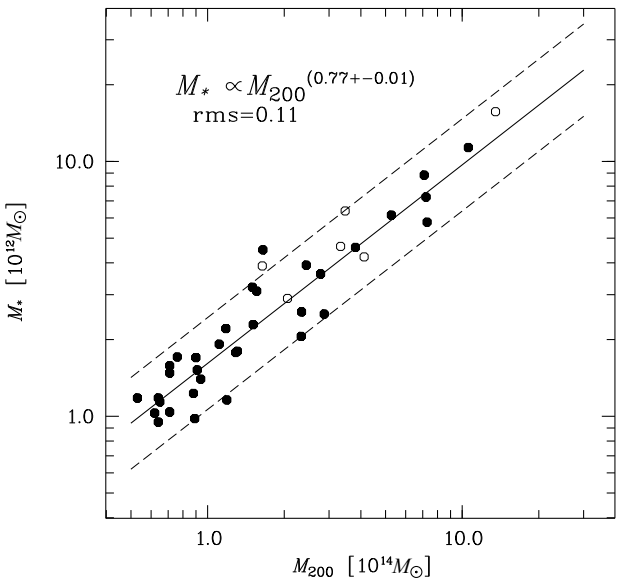

Fig. 5. Dependence of the galaxy cluster stellar mass on the halo mass within R_{200c}. The solid line corresponds to the regression ratio $M_*/M_\odot \propto (M_{200c}/M_\odot)^{0.77\pm0.004}$, and the dashed lines show 2σ deviations from it. The empty circles show the galaxy clusters from [22].

$$\log M_{*,200c} = (1.010 \pm 0.004) \times \log L_{K,200c} - (0.144 \pm 0.050)$$

with a standard deviation of 0.05 (Fig. 4). Masses and luminosities in all the expressions are given in $M_\odot$ and $L_\odot$. Thus, the stellar mass estimates of the galaxies (and in the end, of the galaxy clusters) presented in the SDSS DR10 catalog agree well with their near-IR luminosities. Fig. 5 shows the dependence of the stellar mass of the galaxy systems on their dynamical mass, which we determined from the radial velocity dispersion. The relation has a form of

$$\log M_{*,200c} = (0.77 \pm 0.01) \times (\log M_{200c} - 14.5) + (12.595 \pm 0.12)$$

with standard deviation 0.11 and has shape similar to the one we derived earlier for 182 galaxy systems: $L_{K,200c} \propto M_{200c}^{0.768\pm0.002}$ [21], and also—for 93 galaxy systems: $L_{K,200c} \propto M_{200c}^{0.72\pm0.04}$ [48], and to 55 groups and 6 clusters of galaxies: $L_{K,200c} \propto M_{200c}^{0.64\pm0.06}$ [49].

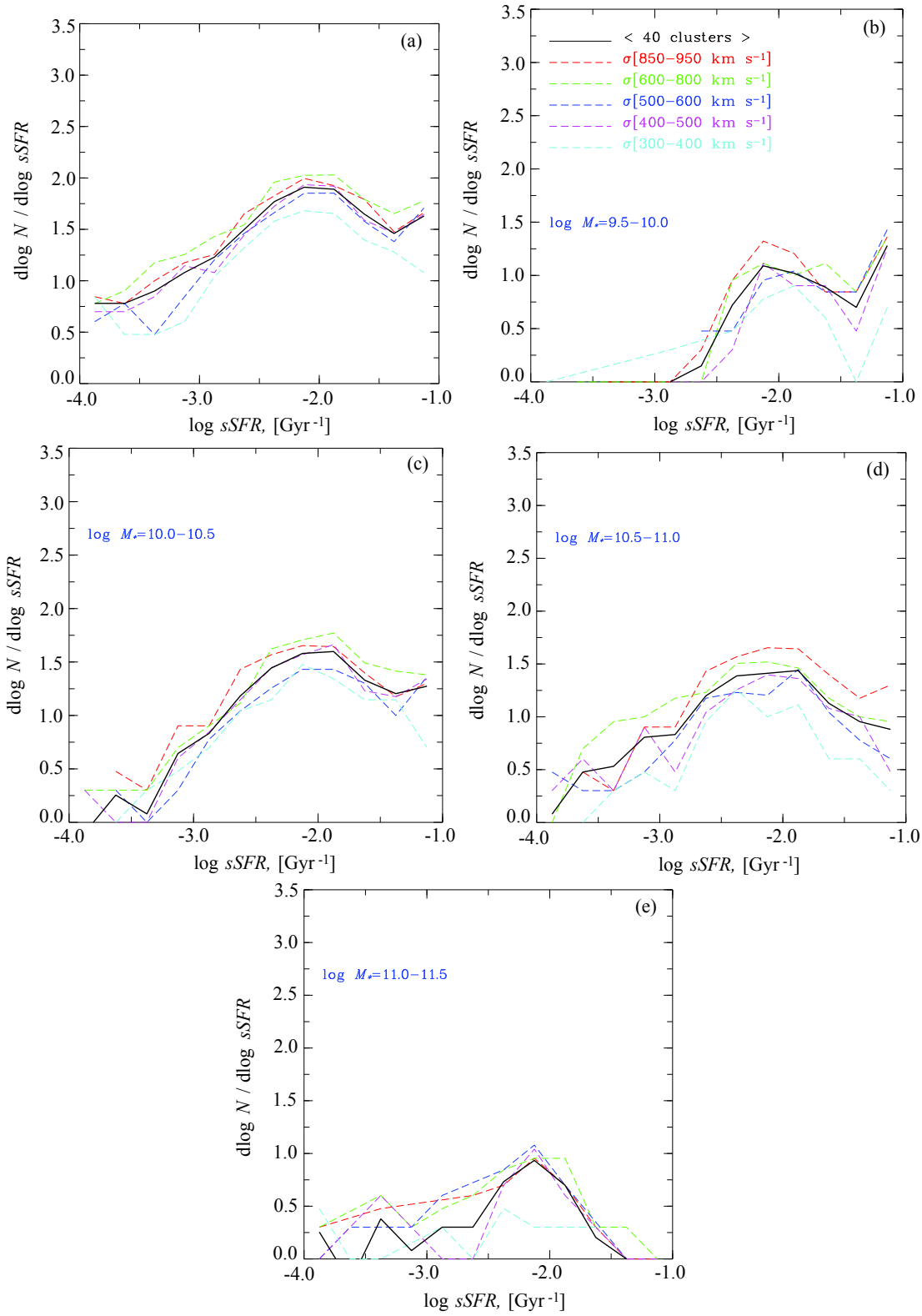

Fig. 6. Distribution of galaxies by their specific star formation rate (log $sSFR$) for the whole sample (a) and with binning by stellar mass (b)–(e). The solid line corresponds to the average value, calculated for all galaxies. Other types of lines show the distributions for groups and clusters of galaxies with the radial velocity dispersion σ in the range of 850–950, 600–800, 500–600, 400–500 and 300–400 km s^{-1}.

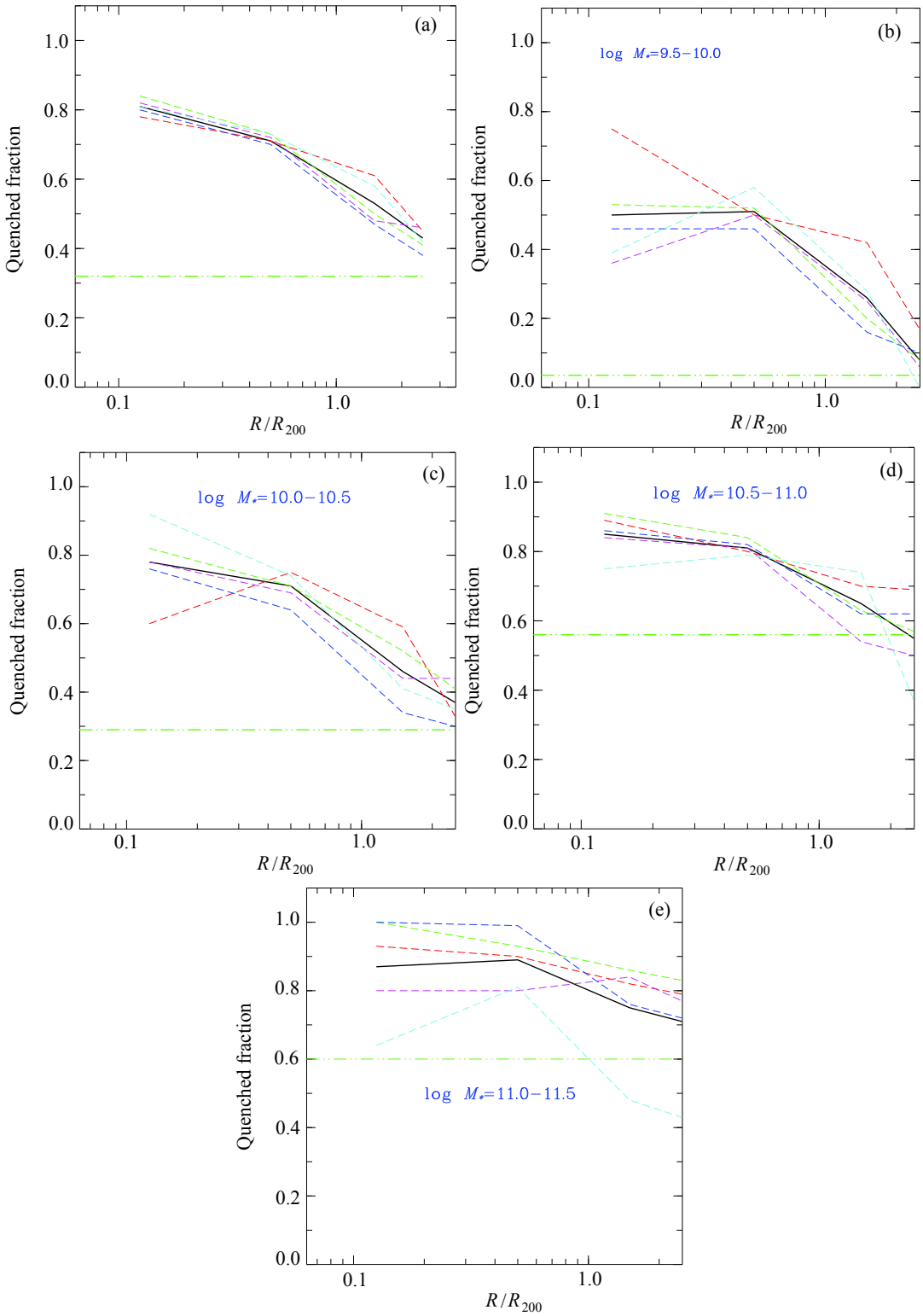

Fig. 7. The fraction of galaxies with quenched star formation ($frac_q$) ($\log sSFR[\mathrm{Gyr}^{-1}] < -1.75$) as a function of distance to the projected cluster center. The clusters are groups in the same way as in the previous figures. The solid line corresponds to the average value for all galaxy systems. Panel (a) shows $frac_q$, found from all the galaxies, panels (b)–(e)—from galaxies binned by stellar mass. In each panel, the dashed-and-dotted line shows the $frac_q$ in the field.

5. SPECIFIC STAR FORMATION RATE IN GROUPS AND CLUSTERS OF GALAXIES

The specific star formation rate ($sSFR$) in a galaxy is determined by the integral star formation rate divided by its stellar mass: $sSFR = SFR/M_*$. The SDSS DR10 catalog gives the results of determining the specific star formation rate as well as the mass of stars in the galaxies. If the conditions $r_{\rm Pet} < 17\overset{\rm m}{.}77$ and $\langle\mu_r\rangle < 24\overset{\rm m}{.}5/\Box''$ are satisfied (the r-band Petrosian magnitude of the galaxy, corrected for galactic extinction, and the average Petrosian surface brightness corresponding to the effective radius), then the completeness of SDSS data is estimated at 99% [50], and 95% for bright galaxies. The missing bright galaxies (mainly early-type with no star formation) within the radius R_{200c} are taken from the NED database, and also derived from the color-magnitude diagrams $(u-r, r, g-r, r, r-i, r)$ [25].

The considered galaxy groups and clusters have radial velocity dispersions σ from 300 to 950 km s^{-1}. We divided that range into the following intervals: 850–950, 600–800, 500–600, 400–500 and 300–400 km s^{-1} and plotted the $\log sSFR$ distributions for all the sample galaxies (Fig. 6a) and with subsample binning according to stellar mass: [9.5; 10.0], [10.0; 10.5], [10.5; 11.0], [11.0; 11.5] $\log M_*[M_\odot]$ (Figs. 6b–6e). Different kinds of lines in Fig. 6 correspond to distributions of galaxies from different radial velocity dispersion intervals.

A minimum is usually found in the $\log sSFR$ distribution which separates the active galaxies from quenched galaxies (QG). A clear bimodality of the distribution and the minimum corresponding to $\log sSFR[\mathrm{yr}^{-1}] = -11$ are found in, e.g., [13] (based on SDSS DR7 data). However, the uncertainties and shifts in SFR measurements for galaxies may create an illusion of bimodality [51], and in order to obtain a single-mode distribution, one must exclude the galaxies with zero star formation rate.

In our case, $\log sSFR[\mathrm{Gyr}^{-1}] \sim -1.5$ or $\log sSFR[\mathrm{yr}^{-1}] \sim -10.5$, correspond to the minimum for the considered clusters (Fig. 6a). We took a common limit for all the systems, equal to $\log sSFR[\mathrm{Gyr}^{-1}] = -1.75$, the same as in our earlier paper [22]. As is evident from Figs. 6b–6e, the $\log sSFR$ distribution has a long tail (left) for systems with the stellar mass in the $\log M_* = [10.5; 11.5]$ interval (QG region), except for the ranges $\log M_* = [10.0; 10.5]$ and especially $\log M_* = [9.5; 10.0]$. The distributions are similar for all the groups and clusters of galaxies in all stellar mass ranges, with the exception of the most low-mass groups with radial velocity dispersions of 300–400 km s^{-1}, where no increase in the number of active galaxies is observed in the $\log M_* = [10.0; 10.5]$ range (Fig. 6c). The distribution has a broad peak $\log sSFR = [-2.3; -1.8]$ for all mass ranges except $\log M_* = [11.0; 11.5]$, where the peak is sharp with the maximum at $\log sSFR \approx -2.2$, with the exception of the low-mass group subsample.

In galaxy clusters the density decreases with increasing distance from the selected center, and the position of a galaxy at a certain radius is related to the time of its entering the cluster (see, e.g., [12]). Fig. 7 shows the fraction of quenched galaxies QG as a function of projected cluster radius normalized to radius R_{200c}. Fig. 7a shows the total fraction of QG without separating by stellar mass, and Figs. 7b–7e show the QG for each stellar mass range individually. Different lines show the variations of the fraction of QG, corresponding to the radial velocity dispersion bin. The total fraction of QG varies from the average value 0.81 ± 0.02 at the distance $(0-0.25)R/R_{200c}$ to 0.43 ± 0.02 at $(2-3)R/R_{200c}$ (or 0.44 ± 0.02 beyond the radius $R_{\rm sp}$). Thus, the fraction of QG decreases at $3R/R_{200c}$ by almost 50%. We found the average (for two fields) fraction of galaxies with quenched star formation, for which the condition $\log sSFR[\mathrm{Gyr}^{-1}] < -1.75$ is met. It is equal to 0.32 ± 0.07, which is 60% less than that in the central regions of the galaxy clusters, or 53% smaller than within the $R_{\rm sp}$ radius, or 26% smaller than within $(2–3)R/R_{200c}$. As is evident from Fig. 7, all σ bins (essentially, bins by mass) show the same behavior along the radius for fixed M_*, except the $\sigma = (300–400)$ km s^{-1} bin (Fig. 7e). For stellar masses in the $\log M_* = [10.5; 11.0]$ range (Fig. 7d), the fraction of QG in the galaxy system outskirts are close to the field values. For the remaining stellar masses (Figs. 7b, 7c and 7e) the QG fraction is higher, on average, than that in the field.

In [12] it is shown for 30 galaxy clusters with $0.15 < z < 0.30$ that the fraction of active galaxies is lower than that in the field even within the radius $3R_{200c}$, i.e., the fraction of QG is higher. According to Wetzel et al. [52], an excess of quenched galaxies is observed beyond the virial radius of the galaxy systems (up to $2.5R_{\rm vir}$), based on SDSS DR7 data. Thus, the fraction of QG remains higher than that in the field even beyond the virialized regions.

Table 3 shows the results of measuring the QG fraction along the normalized cluster radius. The first column in the table gives the system name, the remaining columns give the variation intervals for the radii (R/R_{200c} and $R_{\rm sp}$).

Table 3. Variation of the fraction of quenched galaxies along the radius

Cluster	$(0-0.25)R/R_{200c}$	$(0-1)R/R_{200c}$	$(1-2)R/R_{200c}$	$(2-3)R/R_{200c}$	$(0-1)R_{\rm sp}$	$1R_{\rm sp}-3R/R_{200c}$
(1)	(2)	(3)	(4)	(5)	(6)	(7)
A 2147	0.79 ± 0.36	0.68 ± 0.07	0.54 ± 0.06	0.48 ± 0.05	0.64 ± 0.05	0.49 ± 0.04
A 2063	0.86 ± 0.18	0.71 ± 0.10	0.40 ± 0.10	0.55 ± 0.10	0.66 ± 0.09	0.50 ± 0.08
A 1367	0.74 ± 0.17	0.68 ± 0.09	0.58 ± 0.08	0.39 ± 0.10	0.65 ± 0.08	0.46 ± 0.09
A 2199	0.88 ± 0.20	0.72 ± 0.08	0.60 ± 0.08	0.43 ± 0.07	0.66 ± 0.06	0.43 ± 0.07
A 1185	0.68 ± 0.18	0.56 ± 0.08	0.50 ± 0.09	0.44 ± 0.10	0.55 ± 0.07	0.43 ± 0.08
MKW 03s	1.00 ± 0.30	0.81 ± 0.12	0.56 ± 0.15	0.38 ± 0.15	0.78 ± 0.11	0.40 ± 0.12
NGC 6338	0.84 ± 0.29	0.65 ± 0.14	0.52 ± 0.18	0.60 ± 0.16	0.61 ± 0.12	0.60 ± 0.15
NGC 6107	0.80 ± 0.27	0.83 ± 0.15	0.61 ± 0.18	0.34 ± 0.11	0.75 ± 0.12	0.40 ± 0.10
RXC J1722	0.86 ± 0.33	0.63 ± 0.15	0.41 ± 0.18	0.33 ± 0.17	0.62 ± 0.14	0.33 ± 0.14
MKW 04	0.87 ± 0.33	0.85 ± 0.20	0.25 ± 0.28	0.27 ± 0.18	0.81 ± 0.20	0.25 ± 0.16
UGC 04991	0.50 ± 0.22	0.56 ± 0.14	0.45 ± 0.24	0.20 ± 0.13	0.59 ± 0.14	0.22 ± 0.11
A 1983	0.80 ± 0.24	0.78 ± 0.13	0.49 ± 0.12	0.43 ± 0.17	0.71 ± 0.10	0.42 ± 0.12
MKW 08	0.92 ± 0.38	0.89 ± 0.13	0.54 ± 0.13	0.55 ± 0.16	0.78 ± 0.13	0.56 ± 0.14
NGC 5098	0.73 ± 0.29	0.72 ± 0.16	0.32 ± 0.11	0.50 ± 0.16	0.60 ± 0.12	0.42 ± 0.12
RBS 858	1.00 ± 0.39	0.79 ± 0.18	0.87 ± 0.33	0.25 ± 0.20	0.79 ± 0.16	0.57 ± 0.25
NGC 2795	0.54 ± 0.28	0.52 ± 0.16	0.50 ± 0.23	0.57 ± 0.21	0.53 ± 0.15	0.53 ± 0.16
MKW 04s	1.00 ± 0.63	0.73 ± 0.20	0.62 ± 0.36	0.50 ± 0.43	0.70 ± 0.18	0.60 ± 0.44
VV 196	0.83 ± 0.36	0.56 ± 0.19	0.12 ± 0.09	0.57 ± 0.25	0.52 ± 0.16	0.35 ± 0.13
RXC J1033	0.83 ± 0.38	0.71 ± 0.17	0.67 ± 0.20	0.33 ± 0.17	0.70 ± 0.14	0.40 ± 0.17
AWM 1	0.75 ± 0.40	0.73 ± 0.20	0.33 ± 0.17	0.67 ± 0.30	0.72 ± 0.20	0.48 ± 0.17
AWM 4	1.00 ± 0.53	0.83 ± 0.24	0.44 ± 0.25	0.33 ± 0.22	0.82 ± 0.23	0.28 ± 0.16
NGC 7237	1.00 ± 0.45	0.81 ± 0.20	0.71 ± 0.30	0.50 ± 0.43	0.80 ± 0.17	0.40 ± 0.33
NGC 3158	0.77 ± 0.32	0.68 ± 0.23	0.62 ± 0.36	–	0.69 ± 0.21	0.60 ± 0.44
RXC J1511	0.86 ± 0.48	0.75 ± 0.23	0.46 ± 0.24	0.46 ± 0.24	0.71 ± 0.21	0.44 ± 0.19
NGC 5171	0.54 ± 0.25	0.61 ± 0.17	0.56 ± 0.23	0.30 ± 0.20	0.61 ± 0.14	0.27 ± 0.18
NGC 3119	0.78 ± 0.39	0.73 ± 0.22	0.26 ± 0.13	0.20 ± 0.22	0.62 ± 0.18	0.25 ± 0.14
A 1228B	0.93 ± 0.36	0.80 ± 0.24	0.56 ± 0.22	0.50 ± 0.27	0.74 ± 0.18	0.47 ± 0.21
A 2162	0.88 ± 0.45	0.77 ± 0.25	0.71 ± 0.30	0.50 ± 0.31	0.83 ± 0.23	0.43 ± 0.21
NGC 2783	0.50 ± 0.31	0.56 ± 0.23	0.60 ± 0.44	1.00 ± 0.63	0.56 ± 0.22	0.88 ± 0.45
A 1177	0.75 ± 0.40	0.86 ± 0.28	0.80 ± 0.38	0.50 ± 0.43	0.86 ± 0.24	0.57 ± 0.36
NGC 6098	1.00 ± 0.82	0.50 ± 0.27	0.20 ± 0.22	–	0.36 ± 0.19	0.50 ± 0.61
UGC 07115	0.67 ± 0.43	0.77 ± 0.21	0.71 ± 0.42	0.50 ± 0.31	0.75 ± 0.19	0.50 ± 0.27
NGC 2832	0.88 ± 0.45	0.88 ± 0.26	0.85 ± 0.28	0.90 ± 0.41	0.85 ± 0.21	0.94 ± 0.34
NGC 5627	0.86 ± 0.48	0.74 ± 0.26	0.60 ± 0.31	0.17 ± 0.18	0.77 ± 0.24	0.20 ± 0.15
Total sample ($N = 40$)	0.81 ± 0.02	0.71 ± 0.02	0.53 ± 0.02	0.43 ± 0.02	0.68 ± 0.02	0.44 ± 0.02

6. CONCLUSIONS

The observational data show that galaxies in groups and clusters differ from field galaxies. The existing correlation between the morphology of the galaxies and the density of their outskirts region becomes the morphology—radius ratio in galaxy clusters, since the density decreases with increasing radius. In this work, we investigated the central regions and nearest outskirts of galaxy systems (up to $3R_{200c}$ in projection). For the considered galaxy cluster sample we determined: the specific star formation rate, the quenched galaxy fraction, the fraction of early type galaxies on the "red sequence" in comparison with the field data. We also found for each galaxy system the stellar mass within the R_{200c} radius and compared it with the halo mass, measured from the radial velocity dispersion. The characteristics of 34 galaxy systems from the studied sample are presented in this paper, and the results for six systems have been published earlier [22].

We obtained the following results for all 40 systems:

1. For the considered galaxy systems ($\log M_{200c}/M_\odot = [13.7; 15.00]$) the galaxy stellar mass within the radius R_{200c}, determined from SDSS DR10 data, corresponds to the IR-luminosity measured from the 2MASX data: $M_{*,200c}/M_\odot \propto (L_{K,200c}/L_\odot)^{1.010}$. The dependence between the stellar mass and the dynamical mass (halo) of the system has the form of

$$\begin{aligned}\log M_{*,200c}/M_\odot &= (0.77 \pm 0.01) \\ &\times (\log M_{200c}/M_\odot - 14.5) \\ &+ 12.60 \pm 0.10.\end{aligned}$$

2. A radial gradient of $sSFR$ is present in the galaxy clusters. The fraction of QG is maximal ($\log sSFR[\mathrm{Gyr}^{-1}] < -1.75$) in the central regions and, based on the average for all groups and clusters, amounts to 0.81 ± 0.02 beyond $R_{\rm sp}$ (within $(2-3)R/R_{200c}$)—0.44 ± 0.03. This value, obtained for the outskirts of the galaxy clusters is higher than that in the field by about 27%. The highest variations of the quenched galaxy fraction with radius are observed in galaxy systems with stellar masses of $\log M_*/M_\odot = 9.5$–10.0.

3. The "red sequence" of early type galaxies with small scatter is the main property of galaxy clusters, since bright early type galaxies constitute 60–70% of their virialized regions. We show that $frac_E$ beyond $R_{\rm sp}$ (up to $(2-3)R/R_{200c}$) becomes the same as that in the field.

ACKNOWLEDGMENTS

This research has made use of the NASA/IPAC Extragalactic Database (NED, `http://nedwww.ipac.caltech.edu`), which is operated by the Jet Propulsion Laboratory, California Institute of Technology, under contract with the National Aeronautics and Space Administration, Sloan Digital Sky Survey (SDSS, `http://www.sdss.org`), which is supported by Alfred P. Sloan Foundation, the participant institutes of the SDSS collaboration, National Science Foundation, and the United States Department of Energy and Two Micron All Sky Survey (2MASS, `http://www.ipac.caltech.edu/2mass/releases/allsky/`).

CONFLICT OF INTEREST

The authors declare no conflict of interest.

REFERENCES

1. A. Dressler, Astrophys. J. **236**, 351 (1980).
2. M. L. Balogh, I. K. Baldry, R. Nichol, et al., Astrophys. J. **615**, L101 (2004).
3. G. Kauffmann, C. D. M. White, T.M. Heckman, et al., Monthly Notices Royal Astron. Soc. **353**, 713 (2004).
4. S. Mahajan, G. A. Mamon, and S. Raychaudhury, Monthly Notices Royal Astron. Soc. **418**, 2816 (2011).
5. J. D. Hernádez-Fernádez, J. D. Haines, A. Diaferio, et al., Monthly Notices Royal Astron. Soc. **438**, 2186 (2014).
6. A. Muzzin, R. F. J. van den Burg, S. L. McGee, et al., Astrophys. J. **796**, 65 (2014).
7. K. A. Oman, M. J. Hudson, and P. S. Behroozi, Monthly Notices Royal Astron. Soc. **431**, 2307 (2013).
8. K. A. Oman and M. J. Hudson, Monthly Notices Royal Astron. Soc. **463**, 3083 (2016).
9. J. Rhee, R. Smith, H. Choi, et al., arXiv:1704.04243 (2017).
10. M. L. Balogh, S. L. Morris, H. K. C. Yee, et al., Astrophys. J. **527**, 54 (1999).
11. M. L. Balogh, J. F. Navarro, and S. L. Morris, Astrophys. J. **540**, 113 (2000).
12. C. P. Haines, M. J. Pereira, G. P. Smith, et al., Astrophys. J. **775**, 126 (2015).
13. A. R. Wetzel, J. L. Tinker, and C. Conroy, Monthly Notices Royal Astron. Soc. **424**, 232 (2012).
14. S. P. D. Gill, A. Knebe, and B. K. Gibson, Monthly Notices Royal Astron. Soc. **356**, 1327 (2005).
15. B. R. McNamara and P. E. J. Nulsen, Annual Rev. Astron. Astrophys. **45**, 117 (2007).
16. K. Bekki, W. J. Couch, and Y. Shioya, Astrophys. J. **577**, 651 (2002).
17. J. E. Gunn and J. R. I. Gott, Astrophys. J. **176**, 1 (1972).
18. V. Quilis, B. Moore, and R. Bower, Science **288**, 1617 (2000).

19. A. I. Zabludoff and J. S. Mulchaey, Astrophys. J. **496**, 39 (1998).
20. D. Olave-Rojas, P. Cerulo, R. Demarco, et al., arXiv:1806.08435 (2018).
21. F. G. Kopylova and A. I. Kopylov, Astrophysical Bulletin **70**, 123 (2015).
22. F. G. Kopylova and A. I. Kopylov, Astrophysical Bulletin **73**, 267 (2018).
23. C. P. Ahn, R. Alexandroff, C. Allende Prieto, et al., Astrophys. J. Suppl. **211**, 17 (2014).
24. T. H. Jarrett, T. Chester, R. Cutri, et al., Astrophys. J. **119**, 455 (1997).
25. F. G. Kopylova, Astrophysical Bulletin **68**, 253 (2013).
26. F. G. Kopylova and A. I. Kopylov, Astronomy Letters **39**, 3 (2013).
27. A. I. Kopylov and F. G. Kopylova, Astrophysical Bulletin **70**, 243 (2015).
28. G. A. Mamon, T. Sanchis, E. Salvador-Sole, and M.J. Solanes, Astron. and Astrophys. **414**, 445 (2004).
29. V. R. Eke, S. Cole, and C. S. Frenk, Monthly Notices Royal Astron. Soc. **282**, 263 (1996).
30. S. More, B. Diemer, and A. V. Kravtsov, Astrophys. J. **810**, 36 (2015).
31. B. Tully, Astron. J. **149**, 54 (2015).
32. S. More, H. Miyatake, M. Takada, et al., Astrophys. J. **825**, 39 (2016).
33. C. Chang, E. Baxter, B. Jain, et al., Astrophys. J. **864**, 83 (2018).
34. A. Raichoor and S. Andreon Astron. and Astrophys. **570**, A123 (2014).
35. M. D. Gladders, O. Lopez-Cruz, H. K. C. Yee, and T. Kodama, Astrophys. J. **501**, 571 (1998).
36. B. Garilli, D. Bottini, D. Maccagni, et al., Astrophys. J. Suppl. **105**, 191 (1996).
37. M. Scodeggio, Astron. J. **121**, 2413 (2001).
38. O. Lòpez-Cruz, W. A. Barkhouse, and H. K. C. Yee, Astrophys. J. **614**, 679 (2004).
39. A. Aragon-Salamanca, R. S. Ellis, and R. M. Sharples, Monthly Notices Royal Astron. Soc. **248**, 128 (1991).
40. S. A. Stanford, P. R. M. Eisenhardt, and M. Dickinson, Astrophys. J. **492**, 461 (1998).
41. P. G. van Dokkum, M. Franx, D. Fabricant, et al., Astrophys. J. **541**, 95 (2000).
42. J. P. Blakeslee, Astrophys. J. **596L**, 143 (2003).
43. S. Andreon and M. Huertas-Company, Astron. and Astrophys. **526**, A11 (2011).
44. G. A. Mamon, A. Biviano, and G. Murante, Astron. and Astrophys. **520**, A30 (2010).
45. S. Barsanti, M. S. Owers, S. Brough, et al., arXiv:1803.05076 (2018).
46. C. Conroy, J. E. Gunn, and M. White, Astrophys. J. **699**, 486 (2009).
47. M. Bernardi, A. Meert, R. K. Sheth, et al., Monthly Notices Royal Astron. Soc. **436**, 697 (2013).
48. Y.-T. Lin, J. J. Mohr, and S. A. Stanford, Astrophys. J. **610**, 745 (2004).
49. M. Ramella, W. Boschin, M. Geller, et al., Astron. J. **128**, 2022 (2004).
50. M. A. Strauss, D. H. Weinberg, R. H. Lupton, et al., Astron. J. **124**, 1810 (2002).
51. R. Feldmann, Monthly Notices Royal Astron. Soc. **470**, L59 (2017).
52. A. R. Wetzel, J. L. Tinker, C. Conroy, et al., Monthly Notices Royal Astron. Soc. **439**, 2687 (2014).

Translated by E. Chmyreva